Optics Communications 293 (2013) 116–118

Contents lists available at SciVerse ScienceDirect

Optics Communications

journal homepage: www.elsevier.com/locate/optcom

A mid-IR source with increased bandwidth using tapered As_2S_3 chalcogenide photonic crystal fibers

J. Hu [a,*], C.R. Menyuk [b], L.B. Shaw [c], J.S. Sanghera [c], I.D. Aggarwal [d]

[a] Department of Electrical and Computer Engineering, Baylor University, One Bear Place #97356, Waco, TX 76798, USA
[b] Department of Computer Science and Electrical Engineering, University of Maryland at Baltimore County, Baltimore, MD 21250, USA
[c] Naval Research Laboratory, Code 5620, Washington, DC 20375, USA
[d] Sotera Defense Solutions, 2200 Defense Highway, Crofton, MD 21114, USA

ARTICLE INFO

Article history:
Received 17 September 2012
Received in revised form
7 November 2012
Accepted 7 November 2012
Available online 27 November 2012

Keywords:
Supercontinuum generation
Tapered fiber
Chalcogenide photonic crystal fiber

ABSTRACT

We present simulation results for supercontinuum generation using tapered As_2S_3 chalcogenide photonic crystal fibers (PCFs). We demonstrate that an increased soliton self-frequency shift can be achieved using a tapered PCF. There is an optimal tapered PCF, which yields an additional 0.4 μm shift to longer wavelengths relative to the shift that is obtained in an untapered PCF, leading to an increase in the bandwidth from 2.5 μm to 3.6 μm. However, the ratio of the output power in the region between 3 and 5 μm to the input power decreases in a tapered fiber because of the increased fiber leakage loss.

1. Introduction

Mid-infrared (IR) light has a wide variety of military, medical, and sensing applications [1]. Supercontinuum generation uses the Kerr effect and the Raman effect in optical fibers to broaden the bandwidth of an optical signal, which can be used in combination with chalcogenide or tellurite optical fibers to generate light in the mid-IR region [2]. Mid-IR supercontinuum generation by using bismuth and tellurite photonic crystal fiber (PCF) has been demonstrated [3,4]. However, bismuth and tellurite glass have high loss above 3 μm [3,4]. The amount of power generated in the wavelength range between 3 μm and 5 μm using a pump source at a wavelength of 1.55 μm or 2 μm is less than 5% [3,4]. Chalcogenide glass offers a unique set of properties among optical glasses that make them an excellent choice for mid-IR science and nonlinear optics [5]. The nonlinear refractive indices of As_2S_3 and As_2Se_3 chalcogenide glasses are one order higher than that of bismuth glass [3]. In Refs. [6–10], it was demonstrated that it is possible to use chalcogenide waveguides or fibers to generate a supercontinuum that extends out to 2 μm with a pump at 1.55 μm.

In prior work, we showed that with a fiber laser pump at a wavelength of 2 μm [11–13] more than 25% of the input power can be shifted into the region between 3 μm and 5 μm using an As_2S_3 chalcogenide PCF [14]. The strength of the nonlinearity and the breadth of the anomalous dispersion regime both contribute to the large amount of power that can be obtained between 3 μm and 5 μm relative to what is possible in other fibers.The anomalous dispersion regime for As_2S_3 chalcogenide PCF can extend from 2 μm to 6 μm [14], while Fig. 5 in Ref. [3] shows that the anomalous dispersion regime ranges from 1.5 μm to 3 μm in bismuth-glass fiber, so that it is only possible to generate a small amount of power in the mid-IR wavelength region. In a prior brief meeting report, we showed that an increased soliton self-frequency shift (SSFS) can be achieved using tapered PCF [15]. In this letter we give a detailed prescription for how to further shift the soliton into the IR region using tapered As_2S_3 chalcogenide PCF, leading to an increase in the final bandwidth. In our simulation, we shift the central wavelength in the generalized nonlinear Schrödinger equation to speed up the simulation and save memory in both the time and frequency domains.

2. Theoretical model

We model the light generation in tapered PCF in two stages. In the first stage, we determine the total dispersion in the fiber, given the material dispersion and PCF geometry. The refractive index of the As_2S_3 chalcogenide glass was measured at the Naval Research Laboratory by ellipsometry [16]. The PCF has five layers of air holes in a hexagonal structure with one hole missing in the center. We set the ratio of the hole diameter to pitch, d/Λ, to 0.4, so that the fiber is single-mode [17,18]. We calculated the

* Corresponding author. Tel.: +1 254 710 1853; fax: +1 254 710 3010.
E-mail address: jonathan_hu@baylor.edu (J. Hu).

0030-4018/$ - see front matter © 2012 Elsevier B.V. All rights reserved.
http://dx.doi.org/10.1016/j.optcom.2012.11.021

effective index using COMSOL Multiphysics, a commercial full-vector mode solver based on the finite-element method. We then used the effective index to calculate the total dispersion, which includes waveguide dispersion and material dispersion. In the second stage, we solve the generalized nonlinear Schrödinger equation [17,2].

$$\frac{\partial A(z,t)}{\partial z}+\frac{a}{2}A-i\mathrm{IFT}\{[\beta(\omega_0+\Omega)-\beta(\omega_0)-\Omega\beta_1(\omega_0)]\tilde{A}(z,\Omega)\} = i\gamma\left(1+\frac{i}{\omega_0}\frac{\partial}{\partial t}\right)\left[A(z,t)\int_{-\infty}^{t}R(t-t')|A(z,t')|^2\,dt'\right], \quad (1)$$

where $A(z,t)$ is the electric field envelop, IFT{} stands for the inverse Fourier transform, $\gamma=n_2\omega_0/(cA_{\mathrm{eff}})$ is the nonlinear coefficient, n_2 is the nonlinear refractive index, a is fiber loss, and A_{eff} is the fiber's effective area. The quantity $\beta_1(\omega_0)$ is the first derivative of $\beta(\omega_0)$ with respect to the frequency. We use the full dispersion curve in Eq. (1), which is equivalent to expanding the dispersion relation in a Taylor series when the series converges [17]. The detailed dispersion curves for this fiber have been shown in Ref. [14]. We set the length of the fiber to be 0.5 m. Due to fiber attenuation, the power is too low beyond 0.5 m for the SSFS to continue to operate, and there is no increase in the bandwidth; the power spectrum just attenuates linearly. The input pump wavelength is set as 2 μm with an input FWHM of 500 fs and a peak power of 1 kW. These parameters are similar to what we used in Ref. [14]. We use the same parameters as in Ref. [14] for the Raman response function, nonlinear refractive index, and fiber material loss. The total loss in the simulation includes fiber material loss and leakage loss.

The principal mechanisms that generate a supercontinuum are soliton fission and the SSFS. Modeling supercontinuum generation usually requires a very large number of points ($N_p>2^{15}$), in the time and frequency discretization [2]. In our simulation, the input light has a center frequency at $\omega_0=2\pi c/\lambda_0$, where $\lambda_0=2$ μm. As the light propagates along the fiber, the SSFS effect will shift the central frequency of each individual soliton to lower frequency [19]. Hence, if one uses the original central frequency ω_0 of the input pulse as the central frequency throughout the whole simulation, the large amount of Fourier components will be on the low-frequency side of the carrier throughout the simulation, while most of the components on the high-frequency side will be nearly zero. In the time domain, individual solitons propagate in the anomalous dispersion region, which means most of the light power propagates in the latter half of the time window. To efficiently use memory in both time and frequency domain and speed up the simulation, we shift the central frequency of the simulation to $\omega_0'=2\pi c/\lambda_0'$, where λ_0' is about 3 μm in our case. By shifting the central frequency in the simulation, we can almost halve the number of points in the time and frequency discretizations. We choose ω_0' so that it is on the original frequency grid in order to obtain exactly the same result as if we continued to use the original central frequency, ω_0. Replacing A by $B\exp(i\Delta\omega t)$ in Eq. (1), we obtain the shifted generalized nonlinear Schrödinger equation:

$$\frac{\partial B(z,t)}{\partial z}+\frac{a}{2}B-i\mathrm{IFT}\{[\beta(\omega_0+\Delta\omega+\Omega')-\beta(\omega_0)-(\Omega'+\Delta\omega)\beta_1(\omega_0)]\tilde{B}(z,\Omega')\} = i\gamma\left(1-\frac{\Delta\omega}{\omega_0}+\frac{i}{\omega_0}\frac{\partial}{\partial t}\right)\left[B(z,t)\int_{-\infty}^{t}R(t-t')|B(z,t')|^2\,dt'\right], \quad (2)$$

3. Enhanced SSFS using tapered PCFs

Tapered PCFs decrease the mode field diameter and increase the nonlinearity, allowing one to compress short pulses and to generate supercontinuum [20–22]. Silica tapered PCFs have been fabricated without the air-hole collapsing [23–25]. Here, we describe the use of tapered PCFs to increase the nonlinearity and thus compensate for the power loss along the propagation to achieve an increased SSFS. We simulate supercontinuum generation in PCFs with a fixed length of 0.5 m and with different tapers. The beginning 0.2 m of the fiber has a uniform pitch of 3 μm. In the following 0.3 m of the fibers, the PCFs are linearly tapered to reduce the pitch. We begin tapering at 0.2 m because there is no significant broadening in an untapered PCF after 0.2 m, as shown later in the paper. The hole diameter to pitch ratio is preserved along the taper, and the PCF remains endlessly single-mode [17,20]. Hence, there is no coupling between the fundamental mode and higher-order modes. In the tapered portion of the PCF, the dispersion and nonlinearity are calculated in accordance with the fiber structure and are used at each step of the split-step Fourier transform [26]. Fig. 1 shows the supercontinuum generation for a central soliton wavelength with the longest wavelength and the ratio of the power generated between 3 μm and 5 μm to the total input power at an input wavelength of 2 μm as a function of the pitch at the end of the tapered PCF. The PCF with a pitch of 3 μm at the end of the PCF is an untapered PCF. As the pitch at the end of the tapered PCF decreases, the center wavelength of the soliton with the longest wavelength increases. However, the ratio between the power generated between 3 μm and 5 μm and the input power decreases. The reason is that the leakage loss increases as the pitch decreases [20]. When the end

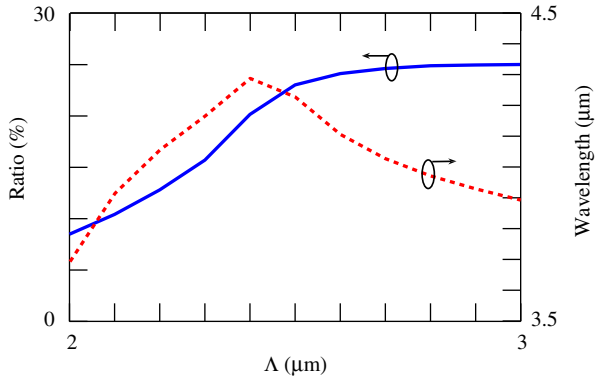

Fig. 1. The central wavelength of the soliton with the longest wavelength and the ratio of the power generated between 3 μm and 5 μm to the total input power as a function of the pitch at the end of the tapered PCF.

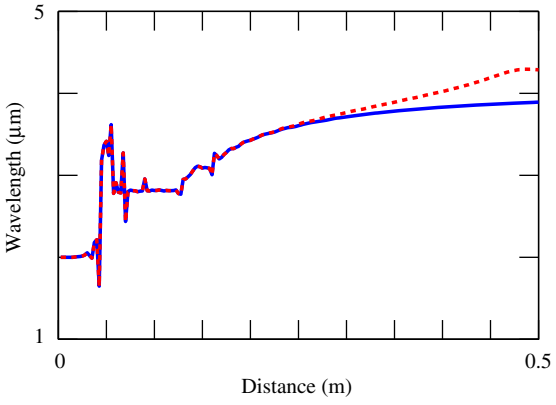

Fig. 2. The central wavelength for the soliton with the longest wavelength. The blue solid and red dashed curves represent the center wavelength using a PCF with a uniform pitch and a tapered PCF with an ending pitch of 2.4 μm, respectively. (For interpretation of the references to color in this figure caption, the reader is referred to the web version of this article.)

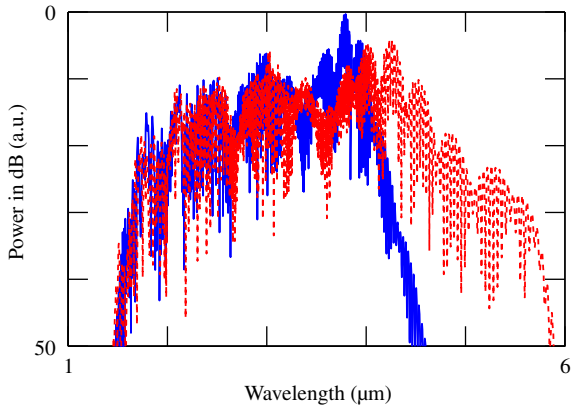

Fig. 3. Spectra at the end of 0.5 m of PCF. The blue solid curve and red dashed curve show the spectra using an untapered PCF and tapered PCF with an ending pitch of 2.4 μm, respectively. (For interpretation of the references to color in this figure caption, the reader is referred to the web version of this article.)

pitch is less than 2.4 μm, the tapering induces excessive leakage loss. Hence, the SSFS is small, and the central soliton wavelength with the longest wavelength decreases as the end pitch decreases. Note also, the anomalous dispersion region decreases as pitch decreases, as shown in Fig. 1 of Ref. [14], which also suggests that a small pitch does not generate a large supercontinuum, and there will be an optimal pitch leading to the largest SSFS. In our case, the optimal pitch is 2.4 μm, while the ratio of the output power between 3 μm and 5 μm to input power is still about 20%. The center wavelength of the soliton using a tapered PCF increases by about 0.4 μm compared to its center wavelength in an untapered PCF. The nonlinearity increases by about 30% at a wavelength of 4 μm as the pitch of the tapered PCF decreases from 3 μm to 2.4 μm, where $B(z,t)$ is the electric field envelope at the center frequency of $\omega_0+\Delta\omega$.

Fig. 2 shows the central wavelength for the soliton with the longest wavelength. The central wavelength for each soliton is calculated by looking at each individual pulse as it propagates. We perform a Fourier transform on the individual pulse to obtain the central wavelength, which is the wavelength at the peak of the spectrum. The blue solid and red dashed curve represent the central wavelength using an untapered PCF and tapered PCF with an ending pitch of 2.4 μm, respectively. Both curves have the same large fluctuation due to soliton fission when the distance is less than 0.2 m. After a distance of 0.2 m, the solitons have shifted away from each other. The blue solid curve for a PCF with a uniform pitch shows a small SSFS. However, the red dashed curve for a tapered PCF shows a continuous strong SSFS after a distance of 0.2 m due to increased nonlinearity. Fig. 3 shows the spectra at the end of 0.5 m of PCF. The blue solid curve and red dashed curve show the spectra using an untapered PCF and tapered PCF with an ending pitch of 2.4 μm , respectively. The blue solid curve has a 20 dB bandwidth (measured from the peak) of 2.5 μm from 1.7 to 4.2 μm. The red dashed curve has a 20 dB bandwidth of 3.6 μm from 1.7 to 5.3 μm. All the solitons experience the enhanced nonlinearity and SSFS due to tapering, which contributes to the increase of the total bandwidth.

4. Conclusions

In summary, we find that using a tapered PCF with an end pitch of 2.4 μm, the center wavelength of the soliton with the longest wavelength shifts an additional 0.4 μm relative to the shift in an untapered PCF. At the same time, the 20 dB bandwidth increases from 2.5 μm to 3.6 μm. However, the ratio of the output to the input power in the spectral region between 3 and 5 μm decreases as the fiber tapers because of fiber leakage loss.

References

[1] J.S. Sanghera, L.B. Shaw, I.D. Aggarwal, IEEE Journal of Selected Topics in Quantum Electronics 15 (2009) 114.
[2] J.M. Dudley, G. Genty, S. Coen, Reviews of Modern Physics 78 (2006) 1135.
[3] J.H.V. Price, T.M. Monro, H. Ebendorff-Heidepriem, F. Poletti, P. Horak, V. Finazzi, J.Y.Y. Leong, P. Petropoulos, J.C. Flanagan, G. Brambilla, X. Feng, D.J. Richardson, IEEE Journal of Selected Topics in Quantum Electronics 13 (2007) 738.
[4] P. Domachuk, N.A. Wolchover, M. Cronin-Golomb, A. Wang, A.K. George, C.M.B. Cordeiro, J.C. Knight, F.G. Omenetto, Optics Express 16 (2008) 7161.
[5] B.J. Eggleton, B. Luther-Davies, K. Richardson, Nature Photonics 5 (2011) 141.
[6] M. El-Amraoui, J. Fatome, J.C. Jules, B. Kibler, G. Gadret, C. Fortier, F. Smektala, I. Skripatchev, C.F. Polacchini, Y. Messaddeq, J. Troles, L. Brilland, M. Szpulak, G. Renversez, Optics Express 18 (2010) 4547.
[7] M.R. Lamont, B. Luther-Davies, D.-Y. Choi, S. Madden, B.J. Eggleton, Optics Express 16 (2008) 14938.
[8] D.-I. Yeom, E.C. Mägi, M.R.E. Lamont, M.A.F. Roelens, L. Fu, B.J. Eggleton, Optics Letters 33 (2008) 660.
[9] A.C. Judge, S.A. Dekker, R. Pant, C.M. de Sterke, B.J. Eggleton, Optics Express 18 (2010) 14960.
[10] D.D. Hudson, S.A. Dekker, E.C. Mgi, A.C. Judge, S.D. Jackson, E. Li, J.S. Sanghera, L.B. Shaw, I.D. Aggarwal, B.J. Eggleton, Optics Letters 36 (2011) 1122.
[11] S.D. Jackson, A. Sabella, D.G. Lancaster, IEEE Journal of Selected Topics in Quantum Electronics 13 (2007) 567.
[12] M. Eichhorn, S.D. Jackson, Optics Letters 33 (2008) 1044.
[13] Q. Wang, J. Geng, T. Luo, S. Jiang, Optics Letters 34 (2009) 3616.
[14] J. Hu, C.R. Menyuk, L.B. Shaw, J.S. Sanghera, I.D. Aggarwal, Optics Letters 35 (2010) 2907.
[15] J. Hu, C.R. Menyuk, L.B. Shaw, J.S. Sanghera, I.D. Aggarwal, in: Proceedings of the Conference on Lasers and Electro-Optics (CLEO), San Jose, CA, paper CThN6, 2009.
[16] H.G. Tompkins, W.A. McGahan, Spectroscopic Ellipsometry and Reflectometry, John Wiley & Sons, Inc., New York, 1999.
[17] J. Hu, C.R. Menyuk, L.B. Shaw, J.S. Sanghera, I.D. Aggarwal, Optics Express 18 (2010) 6722.
[18] G. Renversez, F. Bordas, B.T. Kuhlmey, Optics Letters 30 (2005) 1264.
[19] J.P. Gordon, Optics Letters 11 (1986) 662.
[20] J. Hu, B.S. Marks, C.R. Menyuk, J. Kim, T.F. Carruthers, B.M. Wright, T.F. Taunay, E.J. Friebele, Optics Express 14 (2006) 4026.
[21] A.C. Judge, O. Bang, B.J. Eggleton, B.T. Kuhlmey, E.C. Mgi, R. Pant, C. Martijn de Sterke, Journal of the Optical Society of America B 26 (2009) 2064.
[22] S. Pricking, H. Giessen, Optics Express 18 (2010) 20151.
[23] T.A. Birks, W.J. Wadsworth, P.St.J. Russell, Optics Letters 25 (2000) 1415.
[24] H.C. Nguyen, B.T. Kuhlmey, M.J. Steel, C.L. Smith, E.C. Mägi, R.C. McPhedran, B.J. Eggleton, Optics Letters 30 (2005) 1123.
[25] H.C. Nguyen, B.T. Kuhlmey, E.C. M Agi, M.J. Steel, P. Domachuk, C.L. Smith, B.J. Eggleton, Applied Physics B: Lasers and Optics 81 (2005) 377.
[26] O.V. Sinkin, R. Holzlhner, J. Zweck, C.R. Menyuk, Journal of Lightwave Technology 21 (2003) 61.